NeuroImage 44 (2009) 661–670

Contents lists available at ScienceDirect

NeuroImage

journal homepage: www.elsevier.com/locate/ynimg

A consistent and efficient graphical analysis method to improve the quantification of reversible tracer binding in radioligand receptor dynamic PET studies

Yun Zhou *, Weiguo Ye, James R. Brašić, Andrew H. Crabb, John Hilton, Dean F. Wong

The Russell H. Morgan Department of Radiology and Radiological Science, School of Medicine, Johns Hopkins University, Baltimore, Maryland 21287, USA

ARTICLE INFO

Article history:
Received 8 July 2008
Revised 12 September 2008
Accepted 17 September 2008
Available online 1 October 2008

ABSTRACT

The widely used Logan plot in radioligand receptor dynamic PET studies produces marked noise-induced negative biases in the estimates of total distribution volume (DV_T) and binding potential (BP). To avoid the inconsistencies in the estimates from the Logan plot, a new graphical analysis method was proposed and characterized in this study. The new plot with plasma input and with reference tissue input was first derived to estimate DV_T and BP. A condition was provided to ensure that the estimate from the new plot equals DV_T or BP. It was demonstrated theoretically that 1) the statistical expectations of the estimates from the new plot with given input are independent of the noise of the target tissue concentration measured by PET; and 2) the estimates from the time activity curves of regions of interest are identical to those from the parametric images for the new plot. The theoretical results of the new plot were also confirmed by computer simulations and fifty-five human [^{11}C]raclopride dynamic PET studies. By contrast, the marked noise-induced underestimation in the DV_T and BP images and noise-induced negative bias in the estimates from the Logan plot were demonstrated by the same data sets used for the new plot. The computational time for generating DV_T or BP images in the human studies was reduced by 80% on average by the new plot in contrast to the Logan plot. In conclusion, the new plot is a consistent and computationally efficient graphical analysis method to improve the quantification of reversible tracer binding in radioligand receptor dynamic PET studies.

Introduction

Due to its simplicity, computational efficiency, and readily apparent visual representation of tracer kinetic behavior, a graphical analysis method using the Logan plot (Logan et al., 1990, 1996) has been widely used to characterize and quantify reversible tracer binding in radioligand receptor dynamic PET studies. The Logan plot with plasma input $C_P(t)$ and the Logan plot with reference tissue input $C_{REF}(t)$ are described by Eqs. (1) and (2) below for $t \geq t^*$, respectively,

$$\frac{\int_0^t C(s)ds}{C(t)} = DV_T \frac{\int_0^t C_P(s)ds}{C(t)} + \alpha \quad (1)$$

$$\frac{\int_0^t C(s)ds}{C(t)} = DVR \frac{\int_0^t C_{REF}(s)ds}{C(t)} + \beta \quad (2)$$

where $C_P(t)$ is the tracer concentration in plasma from arterial blood sampling, $C_{REF}(t)$ is the time activity curve (TAC) of reference tissue obtained by applying regions of interest (ROIs) of reference tissue to dynamic images, $C(t)$ is the ROI or pixel-wise TAC of the target tissue tracer concentration measured by PET, DV_T is the tracer total distribution volume in tissue, and DVR is the DV_T ratio of the target to the reference tissues. For the Logan plot with reference tissue input described by Eq. (2), $C(t)/C_{REF}(t)$ is a constant for $t \geq t^*$.

In contrast to classical compartmental modeling techniques, DV_T and DVR estimates obtained by the Logan plot for reversible tracer kinetic binding are independent of specific compartmental model configurations that may differ from tissue to tissue (Koeppe et al., 1991; Gunn et al., 2002; Turkheimer et al., 2003). However, the application of the Logan plot is limited by the noise level of target tissue tracer concentration $C(t)$. There is noise-induced negative bias in the estimates of DV_T and binding potential (BP) (=DVR−1) from the Logan plot, and the underestimation in the estimates from the Logan plot is dependent on both the noise level and magnitude of tissue concentration $C(t)$ (Abi-Dargham et al., 2000; Fujimura et al., 2006; Gunn et al., 2002; Slifstein and Laruelle, 2000; Logan et al., 2001; Wallius et al., 2007). The noise-induced underestimation can result in reduced contrasts in the estimates of BP among targeted tissues, and reduced statistical power to discriminate populations of interest by a specific tissue BP (Zhou et al., 2008). Unfortunately, the $C(t)$ measured by the PET scanning is often accompanied by high noise levels especially when employing pixel-wise tracer kinetic methods. Instead of regular linear regression for the Logan plot, a few numerical

* Corresponding author. The Russell H. Morgan Department of Radiology and Radiological Science, School of Medicine, Johns Hopkins University, 601 N. Caroline Street, JHOC room 3245, Baltimore, MD 21287-0807, USA. Fax: +1 410 955 0696.
E-mail address: yunzhou@jhmi.edu (Y. Zhou).

1053-8119/$ – see front matter © 2008 Elsevier Inc. All rights reserved.
doi:10.1016/j.neuroimage.2008.09.021

methods have been proposed to reduce the noise-induced negative bias but with higher variation in DV_T and BP estimates and higher computational cost (Buchert et al., 2003; Joshi et al., 2007; Varga and Szabo, 2002; Ogden, 2003).

In this study, we first derived an improved graphical analysis method using a new plot with plasma input and with reference tissue input for the quantification of reversible tracer kinetics. The new graphical analysis method was characterized by theoretical analysis, computer simulation, and fifty-five human [^{11}C]raclopride ([^{11}C]RAC) dynamic PET studies. Conventional graphical analysis using the Logan plot was applied to same data sets for comparison. With given input function, the effects of noise in the target tissue concentration $C(t)$ on the estimates from the new and Logan plots were analyzed and evaluated.

Materials and methods

Theory of graphical analysis using a new plot.

New plot with plasma input

The reversible tracer kinetics described by Eq. (3) below is used in the study to derive a new plot with plasma input to estimate DV_T.

$$\frac{dA(t)}{dt} = KA(t) + QC_P(t) \tag{3}$$

Eq. (3) is same as the system equation used in the previous graphical analysis for reversible tracer kinetics (Patlak et al., 1983; Patlak and Blasberg, 1985; Logan et al., 1990, 1996), where $C_P(t)$ is plasma input function, $A(t)=[C_1(t), C_2(t), \ldots C_m(t)]'$, $C_i(t)$ is the tracer concentration in the ith compartment, $'$ is the mathematical transpose operation, K is the system matrix (mxm) and its elements are the transport rate constants between compartments, and Q is a mx1column vector of transport rate constants from vascular space to tissue compartments. For the total tissue tracer concentration $C(t)$ measured by PET, we have $C(t)=\Sigma C_i(t)+V_PC_P(t)=I'A(t)+V_PC_P(t)$, where V_P is the effective plasma volume in tissue, and I is a mx1 column vector of ones. Based on the initial condition $A(0)=[0, 0,\ldots0]'$ (mx1), by substituting the integrated form of Eq. (3) into $\int_0^t C(s)ds = I'\int_0^t A(s)ds + V_P\int_0^t C_P(s)ds$, we have Eq. (4) below,

$$\int_0^t C(s)ds = \left(-I'K^{-1}Q + V_P\right)\int_0^t C_P(s)ds + I'K^{-1}A(t) \tag{4}$$

where K^{-1} is the inverse of matrix K. When the system reaches equilibrium relative to plasma input for $t\geq t^*$, i.e., $C_i(t)=R_iC_P(t)$, $i=1, 2,\ldots m$, for $t\geq t^*$, then, $I'K^{-1}A(t)=I'K^{-1}RC_P(t)=\delta\ C_P(t)$, where $R=[R_1, \ldots R_m]'$, and $\delta=I'K^{-1}R$ is a constant. For the kinetic system described by Eq. (3), $-K^{-1}Q$ is the distribution volume vector $[DV_1,DV_2, \ldots,DV_m]'$, and DV_i is the tracer DV in ith compartment. Therefore, $-I'K^{-1}Q+V_P=\Sigma DV_i+V_P=DV_T$. By dividing both sides of Eq. (4) by $C_P(t)$, we obtain Eq. (5) for $t\geq t^*$ for the new plot with plasma input to estimate DV_T.

$$\frac{\int_0^t C(s)ds}{C_P(t)} = DV_T\frac{\int_0^t C_P(s)ds}{C_P(t)} + \delta \tag{5}$$

An operationally sufficient condition for the new plot

To derive the new plot described by Eq. (5), a sufficient condition on tracer kinetics is given in the above section, i.e., there exists t^* such that the tracer concentrations in all tissue compartments reach equilibrium relative to plasma input for $t\geq t^*$. In general, the sufficient condition is difficult to evaluate and validate without knowing specific compartmental model configurations. However, in practical radioligand receptor dynamic PET studies, the tracer kinetics in tissue can be described by a three-tissue compartment model with metabolite-corrected plasma input: free, nonspecific binding and specific binding compartments (Wong et al., 1986a,b, 1997). Due to limited study time and temporal resolution of PET scanner, the measured tracer kinetics can be fitted well by either one-tissue three-parameter (K_1, k'_2 V_P) compartment model (one compartment including free, nonspecific and specific binding) or two-tissue five-parameter ((A) free plus nonspecific binding compartment, and specific binding compartment in sequential configuration for target tissue with parameters [K_1, k_2, k_3, k_4, V_P]; or (B) free compartment and nonspecific binding compartment in sequential configuration for reference tissue with parameters [K_{1R}, k_{2R}, k_5, k_6, V_P]) model (2T5PCM) with metabolite-corrected plasma input (Koeppe et al., 1991; Huang et al., 1986; Logan et al., 1990; Lammertsma et al., 1996; Zhou et al., 2007a).

For tracer kinetics following the one-tissue or two-tissue compartment model described as above, if there exists a time point, t^*, such that 1) $C_P(t)$ is a mono-exponential decreasing, and 2) $C(t)/C_P(t)$ is constant, for $t\geq t^*$, then the tracer kinetics in all tissue compartments reaches equilibrium relative to plasma. This is a more practical sufficient condition for the new plot that can be easily evaluated by the tracer kinetics measured by dynamic PET. The proof of the operationally sufficient condition for tracer kinetics to attain relative equilibrium status is quite straightforward and is omitted here. Note that it is necessary to verify the sufficient condition for graphical analysis using the new plot. This is because the plot of $\int_0^t C_P(s)ds/C(t)$ versus $\int_0^t C(s)ds/C_P(t)$ could attain a straight line after t^*, while the slope may not be equal to the DV_T if $I'K^{-1}A(t)/C_P(t)$ is not constant for $t\geq t^*$. In other words, even if $\int_0^t C_P(s)ds/C_P(t)$ versus $\int_0^t C(s)ds/C_P(t)$ attains a straight line after t^*, we cannot imply the constancy of ratio of $I'K^{-1}A(t)$ to $C_P(t)$ for $t\geq t^*$.

New plot with reference tissue input

Assuming the relative equilibrium condition for the new plot with plasma input is validated, and a reference tissue is identified, then we have $C_P(t)=R_PC_{REF}(t)$ for $t\geq t^*$, and Eq. (6) obtained from the Eq. (5) for reference tissue for $t\geq t^*$,

$$\int_0^t C_P(s)ds = \frac{\int_0^t C_{REF}(s)ds - \delta_{REF}C_P(t)}{DV_{REF}} \tag{6}$$

where R_P is a positive constant, DV_{REF} is the DV_T of reference tissue. By substituting $C_P(t)=R_PC_{REF}$, and Eq. (6) into Eq. (5) with simple algebraic operations, the plasma input $C_P(t)$ in Eq. (5) for target tissue can be eliminated as Eq. (7) below for $t\geq t^*$ for the new plot with reference tissue input,

$$\frac{\int_0^t C(s)ds}{C_{REF}(t)} = DVR\frac{\int_0^t C_{REF}(s)ds}{C_{REF}(t)} + \theta \tag{7}$$

where $DVR=DV_T/DV_{REF}$, and $\theta=(\delta-DVR\delta_{REF})R_P$.

Binding potential (BP)

BP is an index of tracer specific binding in radioligand receptor PET studies and is defined as $BP=f_2B'_{max}/K_D$ (Huang et al., 1986; Koeppe et al., 1991; Mintun et al., 1984; Innis et al., 2007), where f_2 is the free fraction of tracer in the free and nonspecific binding compartment, B'_{max} (nM) is the available receptor density for tracer binding, and K_D (nM) is the tracer equilibrium dissociation constant. The BP can be calculated from tracer distribution volume as $BP=DV_{F+NS+SB}/DV_{F+NS}-1$, where $DV_{F+NS+SB}=DV_{F+NS}+DV_{SB}$, DV_{SB} and DV_{F+NS} are the DV of specific binding and DV of free plus nonspecific tracer distribution volume (in mL/mL) in the tissue, respectively. In a reversible ligand-receptor PET study with identified reference tissue, DV_{F+NS} is usually estimated by the DV of reference tissue devoid of tracer specific binding. For graphical analysis with plasma input, BP is estimated as $BP=DV_T/DV_{REF}-1$ by assuming V_P is negligible in comparison to DV_{F+NS} and $DV_{F+NS+SB}$.

Similarly, for graphical analysis with reference tissue input, the BP is estimated as BP=DVR−1 by assuming that the effects of radioactivity from the vascular space contributed to the measured tissue tracer concentration are also negligible. It is worth noting that the above assumption of the negligible V_P or negligible tissue tracer activity contributed from the vascular space usually resulted in the underestimation of BP (Gunn et al., 2001; Lammertsma and Hume 1996, Logan et al., 1996; Zhou et al., 2003).

Consistency in the estimates from the new plot with given input

The following analysis is focused on the effects of noise in the target tissue concentration, $C(t)$, measured by PET on the estimates from the new plot. With given plasma or reference tissue input, the statistical expectations of the estimates from the new plot with regular linear regression, i.e., ordinary linear least square estimates from the new plot, are independent of noise (ε) if the noise of $C(t)$ measured by PET scanning has mean zero (mean(ε)=0). To conveniently derive the conclusion, we first rewrite Eqs. (5) and (7) in a bilinear form as Eqs. (8) and (9) for $t \geq t^*$, respectively.

$$\int_0^t C(s)ds = DV_T \int_0^t C_P(s)ds + \delta C_P(t) \quad (8)$$

$$\int_0^t C(s)ds = DVR \int_0^t C_{REF}(s)ds + \theta C_{REF}(t) \quad (9)$$

Assuming that there are n frames in total for the measured dynamic PET data, that t_i is the middle time of frame i with duration Δt_i, and that there is additive noise ε_i in the measured tissue tracer radioactivity by PET scanner, i.e., $C(t_i)=C_0(t_i)+\varepsilon_i$, where $C_0(t_i)$ is the true (noise free) tissue tracer concentration at frame i. Let M and M_{REF} be the matrices of the measurements of independent variables from plasma inputs and reference tissue input, respectively; Y be the output measurements; $DV_{T\varepsilon}$ and δ_ε be the estimates obtained by applying new plot to the tissue tracer kinetics of noise ε ($\varepsilon=[\varepsilon_1, \varepsilon_2, \ldots, \varepsilon_n]'$); and $E(x)$ be the statistical expectation of random variable x. Then we have

$$M = \begin{bmatrix} \int_0^{t_1^*} C_P(s)ds & C_P(t_1^*) \\ \cdot & \cdot \\ \cdot & \cdot \\ \cdot & \cdot \\ \int_0^{t_n} C_P(s)ds & C_P(t_n) \end{bmatrix}$$

$$M_{REF} = \begin{bmatrix} \int_0^{t_1^*} C_{REF}(s)ds & C_{REF}(t_1^*) \\ \cdot & \cdot \\ \cdot & \cdot \\ \cdot & \cdot \\ \int_0^{t_n} C_{REF}(s)ds & C_{REF}(t_n) \end{bmatrix}$$

$$Y_\varepsilon = \left[\int_0^{t_1^*} C(s)ds, \ldots, \int_0^{t_n} C(s)ds\right]', \text{ and}$$

$$[E(DV_{T\varepsilon})E(\delta_\varepsilon)]' = E\left((M'M)^{-1}M'Y_\varepsilon\right) = (M'M)^{-1}M'E(Y_\varepsilon)$$
$$= (M'M)^{-1}M'\left[\int_0^{t_1^*} E(C(s))ds, \ldots, \int_0^{t_n} E(C(s))ds\right]'$$
$$= (M'M)^{-1}M'\left[\int_0^{t_1^*} C_0(s))ds, \ldots, \int_0^{t_n} C_0(s))ds\right]'$$

$= [DV_T\ \delta]'$. Through similar derivations, we have $[E(DVR_\varepsilon)\ E(\theta_\varepsilon)]' = [DVR\ \theta]'$. This means that with given plasma or reference tissue input, the DV_T and DVR estimates from the new plot with conventional linear regression are consistent for the tissue tracer kinetics of mean zero noise.

As demonstrated below, the BP estimates from the new plot with given plasma or reference tissue input are also consistent for the tissue tracer kinetics of mean zero noise. For the BP estimated by the new plot with reference tissue input, we have $E(BP_\varepsilon)=E(DVR_\varepsilon-1)=E(DVR_\varepsilon)-1=DVR-1=BP$. For the BP calculated through DV_T, it is reasonable to assume that the $DV_{REF\varepsilon}$ is of negligible noise and is approximately equal to DV_{REF}. This is because $DV_{REF\varepsilon}$ is obtained either by applying the new plot to the reference tissue TACs ($DV_T(C_{REF\varepsilon}(t))$ or by applying ROIs of reference tissue to the DV_T images ($DV_{T\varepsilon}$(reference tissue)) generated by the new plot, where both $C_{REF\varepsilon}(t)$ and $DV_{T\varepsilon}$(reference tissue) are of negligible noise level after averaging over all pixels within reference tissue ROIs. Based on the assumption of additive mean zero noise in the dynamic images, and the fact that there is no noise-induced bias in the DV_T images generated by the new plot with given input, we have $C_{REF\varepsilon}(t)=C_{REF}(t)$, $DV_{REF\varepsilon}=DV_T(C_{REF\varepsilon}(t))=DV_T(C_{REF}(t))=DV_{REF}$, and $DV_{REF\varepsilon}=DV_{T\varepsilon}$(reference tissue)$=DV_{REF}$. Therefore, for the BP calculated through the DV_T from the new plot with plasma input, we have $E(BP_\varepsilon)=E((DV_{T\varepsilon}-DV_{REF\varepsilon})/DV_{REF\varepsilon})=E((DV_{T\varepsilon}-DV_{REF})/DV_{REF})=E(DV_{T\varepsilon})/DV_{REF}-1=DV_T/DV_{REF}-1=BP$. Thus, with appropriate assumptions, we have shown theoretically that the statistical expectations of the estimates of DV_T, DVR and BP from the new plot with given input are independent of the noise of target tissue concentration $C(t)$.

Estimates from parametric images equal those from ROI kinetics for the new plot

For the new plot with plasma or reference tissue input, the estimates obtained by applying ROI to parametric images are identical to those obtained from ROI kinetics. This can be seen from following algebraic operation for DV_T:

$$[DV_T(\text{ROI parametric})\ \delta(\text{ROI parametric})]'$$
$$= (\Sigma_j([DV_T(\text{parametric})^j\ \delta(\text{parametric})^j]'))/N$$
$$= (\Sigma_j((M'M)^{-1}M'Y^j))/N = (M'M)^{-1}M'((\Sigma_j Y^j)/N)$$
$$= (M'M)^{-1}M'Y(\text{ROI kinetic})$$
$$= [DV_T(\text{ROI kinetic})\ \delta(\text{ROI kinetic})]',$$

where N is total pixel number of the ROI. By similar derivation for DVR, we have

$$[DVR(\text{ROI parametric})\ \theta(\text{ROI parametric})]'$$
$$= [DVR(\text{ROI kinetic})\ \theta(\text{ROI kinetic})]'.$$

For the BP calculated by DV_T as the $BP=DV_T/DV_{REF}-1$ for the DV_T from the new plot with plasma input, we have BP(ROI parametric)$=DV_T$(ROI parametric)$/DV_{REF}$(parametric)$-1=DV_T$(ROI kinetic)$/DV_{REF}$(kinetic)$-1=$BP(ROI kinetic). For the BP estimated by the new plot with reference tissue input, we have BP(ROI parametric)=DVR(ROI parametric)$-1=$DVR(ROI kinetic)$-1=$BP(ROI kinetic). This means that, for the new plot, the BP estimates obtained by applying ROI to BP images are also identical to those obtained from ROI kinetics. Thus, we have shown theoretically that the estimates of DV_T, DVR, and BP from parametric images are identical to those from ROI kinetics for the new plot.

Computational efficiency

In contrast to the Logan plot, the proposed new plot markedly reduces the computational cost to generate parametric images of DV_T and DVR, and to estimate DV_T and DVR from a set of ROI TACs. This is mainly due to: 1) the regression independent variables for the new plot are same for all pixels or ROI TACs that are determined only by plasma input $C_P(t)$ or reference tissue input $C_{REF}(t)$; and 2) the calculation of linear regression for the new plot can be simultaneously carried on a

large set of pixels or ROI TACs by the product of one matrix determined by regression variables (=$((M'M)^{-1}M')$ or $((M'_{REF}M_{REF})^{-1}M'_{REF})$) and one matrix determined by all pixels or ROI TACs (=$([Y^1,Y^2,\ldots,Y^{nxyz}])$) as follows:

$$[DV_T\ (\text{image})\ \delta(\text{image})]' = ((M'M)^{-1}M')([Y^1,Y^2,\ldots,Y^{nxyz}]), \text{ and}$$
$$[DVR\ (\text{image})\ \theta(\text{image})]' = ((M'_{REF}M_{REF})^{-1}M'_{REF})([Y^1,Y^2,\ldots,Y^{nxyz}]),$$

where M and M_{REF} are regression matrices, $Y^j = \left[\int_0^{t_1^*} c^j(s)ds, \ldots, \int_0^{t_n} c^j(s)ds\right]'$, $C^j(t)$ is the TAC of pixel j, and nxyz is the pixel number of whole image volume. By contrast, for the DV_T and DVR images generated by the Logan plot, the regression variables of $\left[\int_0^t C_P(s)ds/C(t)\ 1\right]$ or $\left[\int_0^t C_{REF}(s)ds/C(t)1\right]$ are dependent on both plasma input $C_P(t)$ or reference tissue input $C_{REF}(t)$ and each pixel or ROI TAC $C(t)$, therefore, the regression matrix and linear regression for the Logan plot need to be calculated in pixel-by-pixel or ROI-by-ROI bases. Obviously, this is not as efficient for a large set of dynamic data, as compared to the new plot.

The derivations and results in the above subsections for the new plot with Eqs. (8) and (9) are also valid for the new plot with Eqs. (5) and (7). This is because 1) the statistical analysis of consistency for the new plot is based on the condition of "with given input" to evaluate the effects of noise in the target tissue concentration $C(t)$; and 2) the above algebraic derivations will be exactly same for the new plot with Eqs. (5) and (7). In addition, as demonstrated numerically in the subsection of "Bilinear form of plots, multilinear and simplified reference tissue model for DVR or BP estimation" in Discussions section, the ROI estimates of DV_T and BP from the new plot with Eqs. (5) and (7) are approximately equal to those from the new plot with its bilinear form using Eqs. (8) and (9).

Human [^{11}C]RAC dynamic PET

Fifty-five human (healthy volunteers, 16 females and 39 males, aged 31.5±9.8 years (mean±SD hereafter for "±"), range (18.0, 55.0) years) [^{11}C]RAC dynamic PET studies with arterial blood sampling for plasma input were used to evaluate the graphical analysis using the new plot. [^{11}C]RAC was used for D_2-like receptor PET imaging, and the cerebellum was identified as a reference tissue (Farde et al., 1986; Wong et al., 1984, 1986a). All dynamic PET studies were performed on a GE Advance scanner. The PET scanning was started immediately after intravenous bolus tracer injection of 18.3±1.9 mCi (range 12.4 to 22.5 mCi) with high specific activity of 6974.8±7100.7 mCi/μmol (range 1193.8 to 55128.0 mCi/μmol) at time of injection of [^{11}C]RAC. Dynamic PET data were collected in 3-D acquisition mode with protocols of 4×0.25, 4×0.5, 3×1, 2×2, 5×4, and 6×5 (60 min total, 24 frames). To minimize head motion during PET scanning, all participants were fitted with thermoplastic face masks for the PET imaging. Ten-minute ^{68}Ge transmission scans acquired in 2-D mode were used for attenuation correction of the emission scans. Dynamic images were reconstructed using filtered back projection with a ramp filter (image size 128×128, pixel size 2×2 mm^2, slice thickness 4.25 mm), which resulted in a spatial resolution of about 4.5 mm full-width at half-maximum (FWHM) at the center of the field of view. The decay-corrected reconstructed dynamic images were expressed in μCi/mL. Structural magnetic resonance images (MRIs) (124 slices with image matrix 256×256, pixel size 0.94×0.94 mm^2, slice thickness 1.5 mm) were also obtained with a 1.5 T GE Signa system for each subject. MRIs were co-registered to the mean of all frames' dynamic PET images using SPM2 with mutual information method. ROIs of caudate, putamen and cerebellum (reference tissue) were manually drawn on the co-registered MRIs.

ROIs defined on MRIs were copied to the dynamic PET images to obtain ROI TACs for kinetic modeling. The [^{11}C]RAC TACs of the caudate, the putamen, and the cerebellum measured by dynamic PET are of typical reversible binding kinetics that follows the 2T5PCM model (Carson et al., 1997; Lammertsma et al., 1996; Logan et al., 1996). To verify the sufficient condition for graphical analysis using our new plot, the t^* was first determined visually from the plots of time t versus mean of $C(t)/C_P(t)$ over all subjects. The plot of time t versus $C(t)/C_P(t)$ with linear regression for $t \geq t^*$ was used to evaluate the constancy of $C(t)/C_P(t)$ for $t \geq t^*$ by performing a statistical T-test on the hypothesis of zero slope of the linear regression. The plot of time t versus the natural logarithm of $C_P(t)$ with linear regression for $t \geq t^*$ was used to evaluate an exponential fitting to $C_P(t)$ for $t \geq t^*$.

The Logan plot using Eqs. (1–2) and the new plot using Eqs. (5) and (7) were applied to ROI TACs to estimate DV_T and BP from ROI tracer kinetics. The parametric images of DV_T and BP were also generated by the new and Logan plots with the same equations used for ROI kinetics. The BP images generated by the new and Logan plots with plasma input were calculated as $DV_T/DV_{REF}-1$, where the DV_{REF} was obtained by applying reference tissue ROIs to the DV_T images. The mean and standard deviation of DV_T and BP within ROIs on parametric images were calculated, and the percent coefficient of variation of ROI estimates from DV_T and BP images were then calculated as 100*mean/SD. For evaluation the computational efficiency, the time used to generate DV_T and BP images for each dynamic PET study was recorded.

Computer simulation study

The objective of the computer simulation study was to characterize the bias of estimates from the new and Logan plots as a function of noise level of tracer kinetics. A two-tissue five-parameter compartment model with metabolite-corrected plasma input (see the subsection of "An operationally sufficient condition for the new plot") was used to fit the measured tissue TACs, and the fitted ROI TACs were used as "true" (noise free) ROI TACs for simulation. Gaussian noise with zero mean and variance $\sigma_i^2 = \alpha C(t_i)\exp(0.693t_i/\lambda)/\Delta t_i$ was added to the ROI kinetics, where $C(t_i)$ is the mean of ROI tracer concentration at frame i, λ (=20.4 min) is the physical half life of the tracer, Δt_i is the length of the PET scanning interval of frame i, and t_i is the midtime of frame i. A series of α values from 0 to 0.16 with step size of 0.01 were used to simulate different noise levels (Zhou et al. 2003). Five hundred realizations for each noise level were obtained to evaluate the statistical properties of the estimates. The estimates obtained by applying graphical analysis to the "true" (noise free, corresponding to α=0) ROI TACs were used as true parameters.

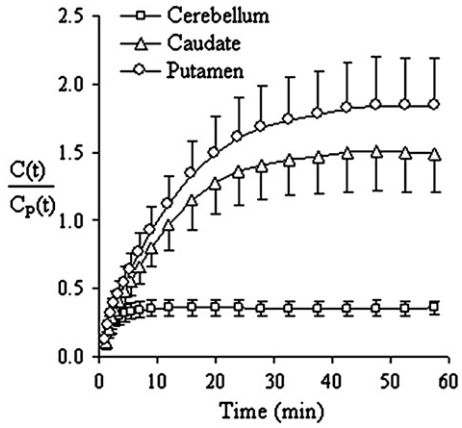

Fig. 1. The mean±standard deviation (n=55) of $C(t)/C_P(t)$ as a function of time post tracer injection. The $C(t)$ is the tissue tracer concentration obtained by applying ROIs (cerebellum, caudate, and putamen) to the reconstructed dynamic images, and $C_P(t)$ is the metabolite-corrected tracer concentration in plasma. The $C(t)/C_P(t)$ approaches to a stable value for $t \geq 42.5$ min for all ROIs.

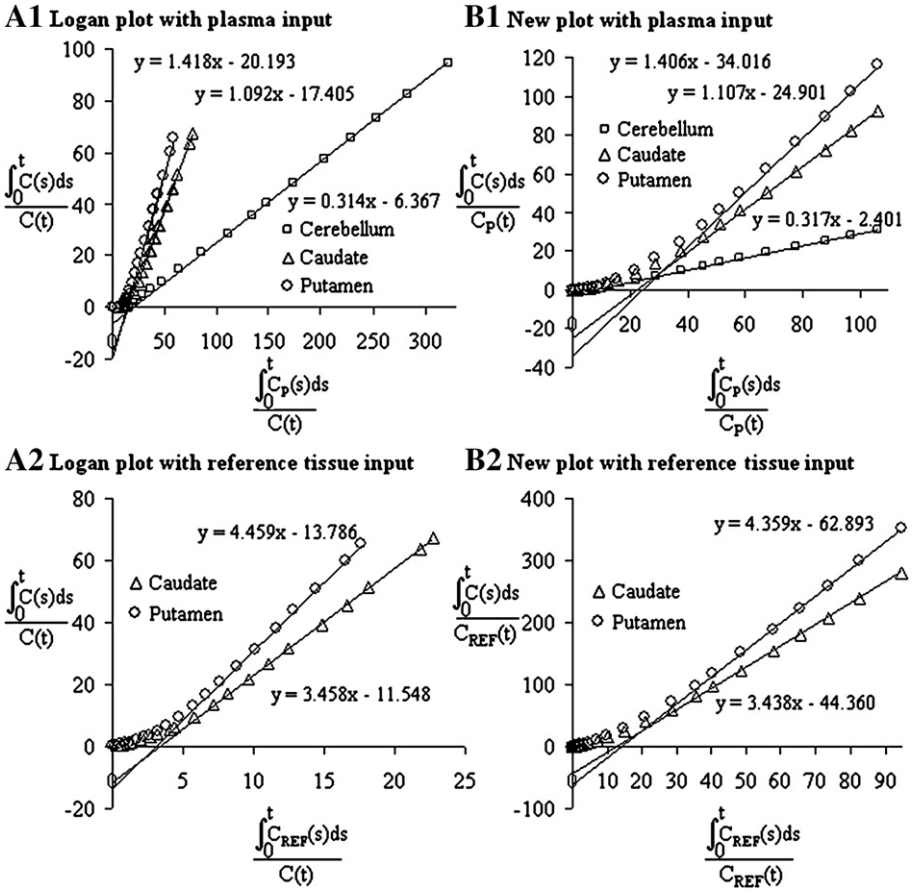

Fig. 2. The Logan and new plots for the time activity curves of the cerebellum, the caudate, and the putamen measured from a typical human [^{11}C]RAC dynamic PET studies. The upper row represents the plots with plasma input to estimate DV_T. The lower row represents the plots with the cerebellar TAC as the reference tissue input to estimate DVR. All plots attained a straight line in the last 4 time points that corresponds the time from 42.5 to 60 min post tracer injection. The slopes of linear regression for the linear portion of last 4 time points from the Logan plot were almost same as those from the new plot.

All parameter estimation methods for ROI kinetic analysis and parametric image generation were written in MATLAB (The MathWorks Inc.) and implemented on a Dell PWS690 workstation.

Results

Sufficient condition for graphical analysis using the new plot

The metabolite-corrected plasma input function was well-fitted by an exponential function for $t \geq 25$ min. The *R*-square of linear regression of time t (independent regression variable) versus the natural logarithm of $C_P(t)$ (dependent regression variable) was $R^2 = 0.983 \pm 0.011$ with the slop of -0.012 ± 0.002 ($n = 55$).

The plot of time t versus mean ± SD of $C(t)/C_P(t)$ in Fig. 1 shows that $C(t)/C_P(t)$ attained a constant for $t \geq t^*$, where $t^* = 25$ min for the cerebellum, and $t^* = 42.5$ min for the caudate and the putamen. The slope of the linear regression of time t versus $C(t)/C_P(t)$ for $t \geq 42.5$ was 0.000 ± 0.001, 0.000 ± 0.006, and 0.002 ± 0.007 ($n = 55$) for the cerebellum, the caudate, and the putamen, respectively. Based on the results from *T*-tests (the *p* values (means ± SD) were 0.386 ± 0.317, 0.392 ± 0.288, and 0.300 ± 0.253 for the cerebellum, the caudate, and the putamen, respectively), the slope was not significantly different from zero.

In conclusion, the sufficient condition for the graphical analysis using the new plot was validated for the ROI kinetics measured from [^{11}C]RAC dynamic PET studies.

New plot versus Logan plot for ROI kinetics

The new and Logan plots with plasma and reference tissue inputs from a representative human [^{11}C]RAC dynamic PET study were demonstrated by Fig. 2. Both new plots and Logan plots attained straight lines in the last 4 points corresponding to the PET scanning time t from 40 to 60 min. The plots with plasma input for the cerebellum approached a line earlier than plots for the caudate and the putamen. This is consistent with the plots of $C(t)/C_P(t)$ in Fig. 1 where the plot of $C(t)/C_P(t)$ for cerebellum attained a constant earlier

Table 1
The means (standard deviations) ($n = 55$) of DV_T and BP estimates from ROI TACs using the Logan plot and the new plot

Parameter	DV_T by plasma input			BP by DV_T		BP by reference tissue input	
ROI	Cerebellum	Caudate	Putamen	Caudate	Putamen	Caudate	Putamen
Logan plot	0.326 (0.047)	1.173 (0.223)	1.432 (0.252)	2.592 (0.379)	3.395 (0.443)	2.607 (0.357)	3.395 (0.426)
New plot	0.325 (0.047)	1.178 (0.218)	1.420 (0.259)	2.615 (0.340)	3.363 (0.397)	2.627 (0.351)	3.381 (0.418)
Paired *T* test	$p = 0.415$, $n = 165$			$p = 0.790$, $n = 110$		$p = 0.820$, $n = 110$	

Notes: The paired two-tailed *T* test was performed between the estimates from the Logan plot and those from new plot. The BP by DV_T was calculated as $BP = DV_T(ROI)/DV_T(cerebellum) - 1$, where the DV_T is estimated by the Logan plot or the new plot with plasma input. There was no significant difference between the estimates from the Logan plot and the new plot for DV_T and BP from ROI TACs.

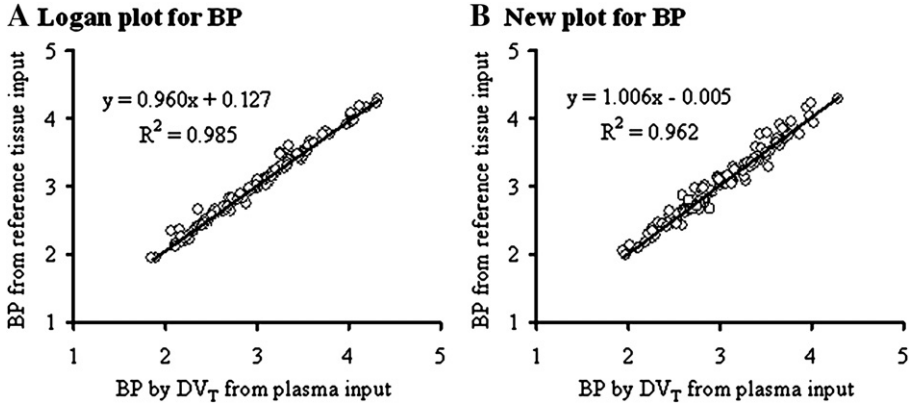

Fig. 3. The correlation between the binding potential (BP) estimates obtained with the DV_T (=DV_T/DV_T(cerebellum) − 1) from graphical analysis with plasma input and those obtained directly by graphical analysis with reference tissue input (=DVR − 1), where the graphical analysis using the Logan plot (Panel A) or the new plot (Panel B) was applied to the TACs of the caudate, the putamen, and the cerebellum(reference tissue) in the fifty-five human [^{11}C]RAC dynamic PET studies. The slope of linear regression in the Panel B for the new plot is not significantly different from 1 (p=0.742).

than the plots of $C(t)/C_P(t)$ for the caudate and the putamen. The slopes of linear regression for the linear portion of last 4 time points from Logan plot were almost same as those from the new plot. Unlike the Logan plot, the x-variable in the new plot is same for all ROIs. The plots demonstrated in Fig. 2 were consistently observed in all 55 human [^{11}C]RAC dynamic PET studies.

The statistics of DV_T and BP estimated from ROI TACs by using the new and Logan plots for all 55 human [^{11}C]RAC dynamic PET studies were summarized in Table 1. There were no significant differences between the estimates of DV_T and BP from the Logan plot and those from the new plot (Table 1). There were no significant differences between the BP estimated from DV_T and those obtained directly by

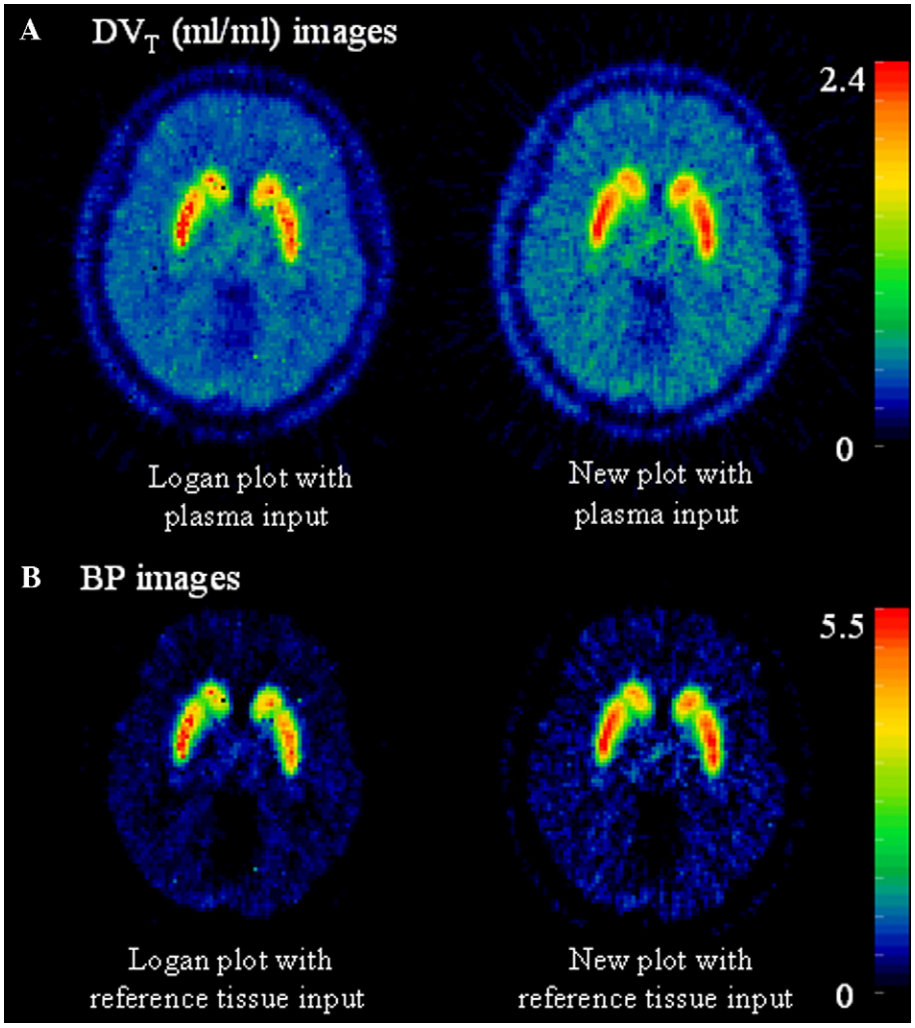

Fig. 4. Transverse parametric images of the total distribution volume (DV_T) and the binding potential (BP) at the level of striatum generated by the Logan plot and the new plot in a representative human [^{11}C]RAC dynamic PET study. The DV_T and the BP from the Logan plot were of higher noise level and significantly lower than those from the new plot.

Table 2
The means (standard deviations) ($n=55$) of ROI estimates from the DV_T and BP parametric images generated by the Logan plot and the new plot

Parameter	DV_T by plasma input			BP by DV_T		BP by reference tissue input	
ROI	Cerebellum	Caudate	Putamen	Caudate	Putamen	Caudate	Putamen
Logan plot	0.302 (0.043)	1.023 (0.192)	1.263 (0.239)	2.382 (0.347)	3.180 (0.447)	2.298 (0.327)	3.047 (0.411)
New plot	0.325 (0.047)	1.178 (0.218)	1.420 (0.259)	2.615 (0.340)	3.363 (0.397)	2.627 (0.351)	3.381 (0.418)
Paired T test	$p<0.0001$, $n=165$			$p<0.0001$, $n=110$		$p<0.0001$, $n=110$	

Notes: The paired two-tailed T test was performed between the estimates from the Logan plot and those from the new plot. The BP by DV_T was calculated as $BP=DV_T/DV_T$ (cerebellum) − 1, where the DV_T was estimated by the Logan plot or the new plot with plasma input, and DV_T(cerebellum) was obtained by applying ROIs of cerebellum on DV_T parametric images. There were significant differences between all estimates from the Logan plot and the new plot for DV_T and BP from parametric images.

using reference tissue input for both the Logan and new plots (paired T-test, $p=0.284$ for the Logan plot, and $p=0.154$ for the new plot). There was a highly linear correlation between the BP values estimated with DV_T and those obtained directly by using reference tissue input for both the Logan and new plots (Fig. 3), and the slope of linear regression for the new plot is not significantly different from 1 (Fig. 3B) ($p=0.742$).

New plot versus Logan plot for parametric images

The DV_T and BP images (Fig. 4) generated by the Logan plot and new plot from a human [^{11}C]RAC dynamic PET study show that the DV_T and BP images generated by the Logan plot were of higher noise levels than those generated by the new plot. The percent coefficients of variation of ROIs (caudate, putamen) on the DV_T images generated by Logan plot were (27.0 ± 3.9, 23.1 ± 5.1) and they were (29.0%, 52.8%) higher than those from the DV_T images generated by the new plot. The percent coefficients of variation of ROIs of (caudate, putamen) on the BP images generated by the Logan plot were (35.6 ± 4.9, 26.6 ± 4.9), and they were (22.1%, 34.3%) higher than those from the BP images generated by the new plot.

The means of ROI estimates from DV_T and BP images generated from the Logan plot and the new plot are listed in Table 2. In contrast to estimates from ROI TACs (see Table 1), the ROI estimates from the DV_T and BP images generated from the Logan plot were significant lower than those from the parametric images generated by the new plot ($p<0.001$).

The computational time utilized to generate DV_T or BP images in the human studies was reduced by 80% on average by the new plot as compared to the Logan plot. Specifically, the computational time utilized for the Logan and new plots with plasma input to generate DV_T images in each dynamic PET study was 44.9 ± 0.9 and 8.8 ± 0.6 s ($n=55$), respectively. To generate whole brain volume BP images, the computational time utilized for the Logan and new plots with reference tissue input were 43.0 ± 1.9 and 8.5 ± 0.4 s ($n=55$), respectively.

Estimates from ROI kinetics versus parametric images

Consistent with the theory described in the Theory section for the new plot, Fig. 5 shows that the estimates of DV_T and BP from ROI kinetics were identical to those obtained by applying ROIs to the DV_T and BP images. However, for the Logan plot, the ROI estimates from DV_T and BP images were significantly lower than those obtained from ROI kinetics (Fig. 6). The percent underestimation in the BP images calculated from DV_T was (7.9%, 6.3%) on average for (caudate, putamen) that was significantly lower (paired T-test, $p<0.001$) than the percent underestimation in the DV_T images (12.7%, 11.9%) and in the BP images (11.8%, 10.3%) generated by the Logan plot using reference tissue input. This is because that the noise-induced percent underestimation in the DV_T images generated by the Logan plot was not consistent across brain tissues, especially between target and reference tissues. For example, Fig. 6 shows that the lowest percent underestimation was observed in the cerebellum reference tissue (7.4% on average) in the DV_T images generated by Logan plot with plasma input.

Simulation study

The noise-induced underestimation or negative bias in the DV_T and BP estimates obtained by the Logan plot in the simulation study is demonstrated by Fig. 7. The noise-induced percent underestimation in the DV_T and BP estimates from the Logan plot increased monotonically to a stable value as the noise level (α) increased. The percent underestimation from true values in the DV_T estimates from the Logan plot in the caudate and the putamen was higher than in the cerebellum. When the noise level α was about 0.02, the percent underestimation in the DV_T and BP estimates in the simulation study (see Fig. 7) was comparable to those observed in the DV_T and BP images generated from human studies where the estimates from low noise level ROI TACs was used as references (see Fig. 6).

For the new plot with given plasma inputs and cerebellum reference tissue inputs from fifty-five human studies, the means of

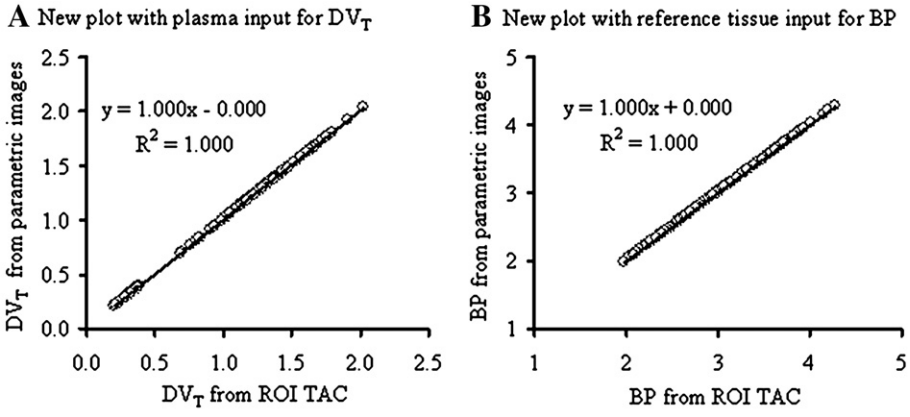

Fig. 5. For the new plot, the total distribution volume (DV_T) and the binding potential (BP) estimated from ROI TACs were identical to those obtained by applying ROIs to the DV_T and BP images.

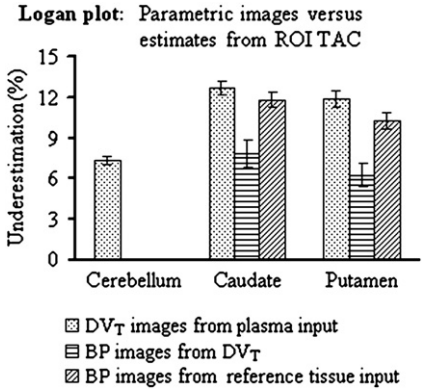

Fig. 6. The percent underestimation in the total distribution volume (DV_T) and the binding potential (BP) images generated by the Logan plot. The estimates from ROI TACs were used as the reference. The BP images from DV_T were calculated as DV_T(image) / DV_T (cerebellum on DV_T image) − 1.

estimates of DV_T and BP over 500 realizations were the same for all noise levels (α from 0 to 0.16). The simulation studies confirmed the theoretical result that the statistical expectations of the estimates from the new plot with given input were independent of the noise of the target tissue concentration measured by PET.

Discussion

Sufficient condition for the new and Logan plots

For the reversible tracer kinetics described by Eq. (4), a sufficient condition for the new graphical analysis is that there is a t^* such that tracer concentration in all compartments attains equilibrium relative to the tracer concentration in plasma, i.e., $C_i(t) = R_i C_P(t)$, $i = 1, 2, \ldots m$, for $t \geq t^*$ (see Theory section). By similar derivation, the condition is also sufficient for classical graphical analysis of the Logan plot described by Eq. (1). Note that the sufficient condition of steady state ($dA/dt = 0$, for $t \geq t^*$) is used to derive graphical analysis using the Logan plot with plasma input (Logan et al., 1990), and this condition is much stronger than the relative equilibrium condition we used in the study for the new plot. Although used to derive the Logan plot with plasma input, the steady state condition is too strong and unnecessary (Logan et al., 1990; Logan, 2003).

In this study, we provided an operational sufficient condition for the new plot. As the results demonstrated in the study, the t^* is usually determined by the plot of time t versus $C(t)/C_P(t)$, where the $C(t)$ is the tracer concentration in the tissue of highest DV_T or BP. This means that the tissue of higher receptor density or higher affinity is usually slower to attain a relative equilibrium state. In addition, the tracer in plasma $C_P(t)$ is usually of fast kinetics and quickly to attain one exponential clearance state.

The effects of the noise in the input function on the new and Logan plots

The effects of noise in the tissue concentration $C(t)$ measured by PET on the new and Logan plots with given input are presented under the Results section. With noise free reference tissue input function $C_{REF}(t)$, there were no noise-induced biases in the estimates from the new plot, but underestimation in the estimates of BP of (caudate, putamen) from the Logan plot increased from 0 to about 12% as noise levels in $C(t)$ from $\alpha = 0$ to 0.02 (see Fig. 7B). To investigate the effects of relatively low noise levels in the input function on the estimates from the new and Logan plots, the reference tissue input was added with a low noise level $\alpha = 0.002$. With a given reference tissue input function $C_{REF}(t)$ of the low noise level, the noise of $C(t)$ induced underestimation in the estimates of BP of (caudate, putamen) from the new plot was minimal ((4.7 ± 3.2)%, (6.0 ± 3.2)%) over all noise levels of $C(t)$, but the underestimation in the estimates of BP from the Logan plot was dependent on the noise level of $C(t)$ and could be as high as ((41.3 ± 3.1)%, (41.8 ± 3.2)%) when $\alpha = 0.02$.

Bilinear form of plots, multilinear and simplified reference tissue model for DVR or BP estimation

The bilinear form of the new plot (Eqs. (8–9)) and the Logan plot (Eqs. (10–11)) were also applied to ROI and pixel-wise tracer kinetics in the fifty-five human [^{11}C]RAC dynamic PET studies.

$$\int_0^t C(s)ds = DV_T \int_0^t C_P(s)ds + \alpha C(t) \quad (10)$$

$$\int_0^t C(s)ds = DVR \int_0^t C_{REF}(s)ds + \beta C(t) \quad (11)$$

As showed by following linear correlations, the ROI estimates of DV_T and BP from the new plot with Eqs. (5) and (7) are almost identical to those from the new plot with its bilinear form using Eqs. (8) and (9).

DV_T(ROI TAC with Eq. (8)) = 0.999DV_T(ROI TAC with Eq. (5)) + 0.000, $R^2 = 1.000$, DV_T(ROI on parametric image with Eq. (8)) = 0.999DV_T(ROI on parametric image with Eq. (5)) + 0.000, $R^2 = 1.000$, BP(ROI TAC with Eq. (9)) = 0.999BP(ROI TAC with Eq. (7)) + 0.003, $R^2 = 1.000$, BP(ROI on parametric image with Eq. (9)) = 0.999BP(ROI on parametric image with Eq. (7)) + 0.003, $R^2 = 1.000$.

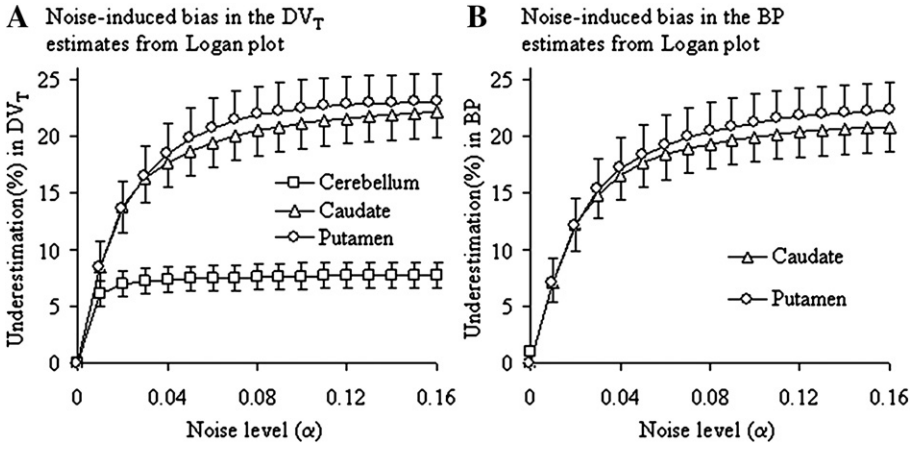

Fig. 7. The mean ± standard error of the percent underestimation in the estimates of total distribution volume (DV_T) and the binding potential (BP) from the Logan plot as function of noise level (α), where the DV_T and the BP estimates from the ROI TACs of noise free were used as true values. The noise-free TACs were the fitted TACs obtained by fitting a two-tissue compartment model to the measured ROI TACs in all fifty-five [^{11}C]RAC human dynamic PET studies.

Similar results for the Logan plot were also obtained as below:

DV_T(ROI TAC with Eq. (10)) = 1.000DV_T(ROI TAC with Eq. (1)) + 0.000, R^2 = 1.000, DV_T(ROI on parametric image with Eq. (10)) = 1.003DV_T(ROI on parametric image with Eq. (1)) −0.001, R^2 = 1.000, BP(ROI TAC with Eq. (11)) = 0.999BP(ROI TAC with Eq. (2)) + 0.003, R^2 = 1.000, BP(ROI on parametric image with Eq. (11)) = 1.002BP(ROI on parametric image with Eq. (2)) + 0.003, R^2 = 1.000.

Based on the consideration of computation cost, and the fact that division is not a stable operation for pixel kinetics at high noise levels, the bilinear form of the new and Logan plots is recommended to generate parametric images of DV_T and BP.

As derived previously (Logan et al., 1996), the Logan plot with Eq. (12) below for $t \geq t^*$ is equivalent to the Logan plot with Eq. (2) when $C(t)/C_{REF}(t)$ is approximately a constant for $t \geq t^*$.

$$\frac{\int_0^t C(s)ds}{C(t)} = DVR\frac{\int_0^t C_{REF}(s)ds + \frac{C_{REF}(t)}{\overline{k'_{2R}}}}{C(t)} + \gamma \quad (12)$$

Results from the human studies consistently demonstrated that the BP estimates from ROI TACs obtained by the Logan plot with Eq. (12) were nearly the same as those obtained by the Logan plot with Eq. (2), where the $\overline{k'_{2R}}$ (1/min) was the mean of k'_{2R} ($=k_{2R}/(1+k_5/k_6)$) estimated from the 2T5PCM model with plasma input. The estimates of k'_{2R} from the human studies was 0.323 ± 0.038 (n = 55) with a range of (0.235, 0.418). Utilizing $\overline{k'_{2R}}$ from 0.2 to 0.5, the BP estimates from ROI TACs of (caudate, putamen) obtained by the Logan plot with Eq. (12) were from (2.599 ± 0.370, 3.397 ± 0.438) to (2.604 ± 0.362, 3.395 ± 0.430) that were almost same as those ((2.607 ± 0.357, 3.395 ± 0.426), see Table 1) from ROI TACs obtained by the Logan plot with Eq. (2).

The DVR or BP can also be estimated by a multilinear reference tissue model (MRTM) (Ichise et al., 1996, 1997) and MRTM with pre-estimated k'_{2R} (MRTM2) (Ichise et al., 2003) in each individual PET study using Eq. (13) for $t \geq t^*$,

$$C(t) = k_2\left(\int_0^t C_{REF}(s)ds + \frac{1}{k'_{2R}}C_{REF}(t)\right) - k'_2\int_0^t C(s)ds \quad (13)$$

where k_2 is the efflux rate constant from free plus nonspecific binding compartment to vascular space, $k'_2 = k_2/DVR$. The DVR or BP (=DVR − 1) is calculated after multilinear regression.

It is important to note that the over or under estimation in the $\overline{k'_{2R}}$ for the Logan plot with Eq. (12) and the k'_{2R} for MRTM2 can result in the biased estimates of DVR or BP if $C(t)/C_{REF}(t)$ is not an approximately constant for $t \geq t^*$. We have demonstrated that the estimates of [^{11}C]methylphenidate BP in the striatum from the Logan plot with Eq. (12) decreased monotonically in $\overline{k'_{2R}}$ (Zhou et al., 2007b). Therefore, to have unbiased $\overline{k'_{2R}}$ or k'_{2R} is critical for appropriate use of Logan plot with Eq. (12) and MRTM2 with Eq. (13) if $C(t)/C_{REF}(t)$ is not an approximately constant for $t \geq t^*$.

Without knowledge of t^*, DVR or BP can also be estimated by using multilinear regression with the following operational equations over the entire PET scan period (Zhou et al., 2003):

$$C(t) = R_1C_{REF}(t) + k_2\int_0^t C_{REF}(s)ds - k'_2\int_0^t C(s)ds \quad (14)$$

$$\int_0^t C(s)ds = DVR\int_0^t C_{REF}(s)ds + \frac{R_1}{k'_2}C_{REF}(t) - \frac{1}{k'_2}C(t) \quad (15)$$

Eqs. (14–15) are derived from a simplified reference tissue model (SRTM) (Zhou et al., 2003), where R_1 is the relative transport rate constant from the vascular space to the tissue space ($=K_1/K_{1R}$). Note that Eq. (14) derived from the SRTM model is same as the Eq. (13) of MRTM, where Eq. (13) can be obtained by substituting $R_1 = k_2/k'_{2R}$ to Eq. (14).

The DVR or BP (=DVR − 1) estimated by Eq. (14) as $DVR = k_2/k'_2$ after regression is not a least square estimate, and the high variance of estimates of k'_2 and k_2 can result in the large error propagation that is associated with division. Results from our previous study showed that the accuracy of DVR estimates from Eq. (14) with conventional multilinear regression can be improved by using Eq. (15) and multilinear regression with a spatial constraint algorithm (Zhou et al., 2003). The noise level of the BP images generated by the SRTM using multilinear regression with Eq. (15) was comparable to those generated by the new plot with reference tissue input in the human [^{11}C]RAC dynamic PET studies. Although the noise-induced bias can be minimized by some numerical algorithms for the bilinear form of the Logan plot, and multilinear form of the SRTM or MRTM, they are all still biased estimators that are dependent on both the noise level and the magnitude of the tracer kinetics.

Computational efficiency of new plot

The computational efficiency of the new plot will be remarkable when the DV_T or BP images are generated from large volume dynamic PET data set. For example, 723.0 ± 11.2 and 208.9 ± 56.4 s were used to generate BP images of whole brain volume from [^{11}C]RAC human dynamic high resolution research tomography (HRRT) studies (n = 10) for the Logan plot and new plot, respectively. The computational efficiency of the new plot is expected to be significant for quantification in the sinogram space. Note that the graphical method using the new plot can be used to generate DV_T and BP images directly from sonogram space.

Patlak plot versus new plot

A graphical analysis approach for the quantification of irreversible tracer kinetics in dynamic PET studies is the well-known as Patlak plot (Gjedde, 1981; Patlak et al., 1983; Patlak and Blasberg, 1985; Wong et al., 1986a). For the Patlak plot, the curve is generated by plotting $\int_0^t C_P(s)ds/C_P(t)$ (x-variable) versus $C(t)/C_P(t)$ (y-variable). Based on the theory of Patlak plot, there exists a time point, t^*, such that the plotted curve reaches a straight line for $t \geq t^*$, and the slope of the linear portion of the curve from t^* to the end of PET scan equals the tissue tracer uptake rate constant K_i.

Although the Patlak plot is used for the quantification of irreversible ligand-receptor binding, the estimates from the Patlak plot have the same statistical properties of the estimates from the new plot demonstrated in the study, i.e., 1) the expectation of K_i estimates from the Patlak plot with a given plasma input is independent of the noise of the tissue concentration $C(t)$ measured by PET; and 2) the estimates of K_i obtained by applying Patlak plot to ROI TACs are identical to those obtained by applying ROIs to the K_i images generated by the Patlak plot. This can be easily obtained by the following bilinear form of the Patlak plot for $t \geq t^*$ with the similar analysis used for the new plot.

$$C(t) = K_i\int_0^t C_P(s)ds + VC_P(t) \quad (16)$$

Note that the regression independent variables $\left(\int_0^t C_p(s)ds\ C_P(t)\right)$ in the Eq. (16) are the same as those in the Eq. (8) of the bilinear form of the new plot. Therefore, the Patlak plot and the new plot have similar computational efficiency for the generation of parametric images by regular linear regression.

In summary, a new graphical analysis was first proposed in this study to estimate DV_T and BP for quantification of [^{11}C]RAC binding. The sufficient condition for the graphical analysis using the new plot was carefully evaluated for the [^{11}C]RAC tracer kinetics measured in human dynamic PET studies. For the DV_T and BP estimates from ROI TACs of low noise level, the Logan plot was comparable to the new plot. Results from theoretical analysis, computer simulations, and fifty-five human [^{11}C]RAC dynamic PET studies showed that 1) with given plasma input or reference tissue input, the expectations of the estimates from the new plot are independent of the noise in the target tissue concentration measured by PET; and 2) the estimates from ROI kinetics were identical to those obtained directly from DV_T and BP images generated by the new plot. Thus, we have shown that the new

plot generates consistent estimates of DV_T and BP for quantification of [^{11}C]RAC binding. By contrast, noise-induced significant underestimation in the DV_T and BP estimates from the Logan plot was demonstrated in both human studies and computer simulation. The noise level of the parametric images of DV_T and BP generated by the Logan plot was significantly higher than those from the new plot. The computational time for generating DV_T or BP images in the human studies was reduced by 80% by the new plot as compared to the Logan plot. In conclusion, the new plot is an improved graphical analysis method for the quantification of the reversible tracer binding in radioligand receptor dynamic PET studies.

Acknowledgments

We thank the cyclotron, PET, and MRI imaging staff of the Johns Hopkins Medical Institutions. This work was supported in part by NIH grants DA00412, MH078175, AA12839, AA012837, and AA10158. Thanks to Mary McCaul and Gary Wand for the kind use some of PET data.

References

Abi-Dargham, A., Martinez, D., Mawlawi, O., Simpson, N., Hwang, D.R., Slifstein, M., Anjilvel, S., Pidcock, J., Guo, N.N., Lombardo, I., Mann, J.J., Van Heertum, R., Foged, C., Halldin, C., Laruelle, M., 2000. Measurement of striatal and extrastriatal dopamine D1 receptor binding potential with [^{11}C]NNC 112 in humans: validation and reproducibility. J. Cereb. Blood Flow Metab. 20 (2), 225–243.

Buchert, R., Wilke, F., van den Hoff, J., Mester, J., 2003. Improved statistical power of the multilinear reference tissue approach to the quantification of neuroreceptor ligand binding by regularization. J. Cereb. Blood Flow Metab. 23 (5), 612–620.

Carson, R.E., Breier, A., Bartolomeis, A.D., Saunders, R.C., Su, T.P., Schmall, B., Der, M.G., Pickar, D., Eckelman, W.C., 1997. Quantification of amphetamine-induced changes in [^{11}C] raclopride binding with continuous infusion. J. Cereb. Blood Flow Metab. 17, 437–447.

Farde, L., Hall, H., Ehrin, E., Sedvall, G., 1986. Quantitative analysis of D2 dopamine receptor binding in the living human brain by PET. Science 231 (4735), 258–261.

Fujimura, Y., Ikoma, Y., Yasuno, F., Suhara, T., Ota, M., Matsumoto, R., Nozaki, S., Takano, A., Kosaka, J., Zhang, M.R., Nakao, R., Suzuki, K., Kato, N., Ito, H., 2006. Quantitative analyses of 18F-FEDAA1106 binding to peripheral benzodiazepine receptors in living human brain. J. Nucl. Med. 47 (1), 43–50.

Gjedde, A., 1981. High- and low-affinity transport of D-glucose from blood to brain. J. Neurochem. 36, 1463–1471.

Gunn, R.N., Gunn, S.R., Cunningham, V.J., 2001. Positron emission tomography compartmental models. J. Cereb. Blood Flow Metab. 21, 635–652.

Gunn, R.N., Gunn, S.R., Turkheimer, F.E., Aston, J.A., Cunningham, V.J., 2002. Positron emission tomography compartmental models: a basis pursuit strategy for kinetic modeling. J. Cereb. Blood Flow Metab. 22 (12), 1425–1439.

Huang, S.C., Barrio, J.R., Phelps, M.E., 1986. Neuroreceptor assay with positron emission tomography: equilibrium versus dynamic approaches. J. Cereb. Blood Flow Metab. 6 (5), 515–521.

Ichise, M., Ballinger, J.R., Golan, H., et al., 1996. Noninvasive quantification of dopamine D2-receptors with iodine-123-IBF SPECT. J. Nucl. Med. 37, 513–520.

Ichise, M., Ballinger, J.R., Vines, D., Tsai, S., Kung, H.F., 1997. Simplified quantification and reproducibility studies of dopamine D2-receptor binding with Iodine-123-IBF SPECT in health subjects. J. Nucl. Med. 38, 31–36.

Ichise, M., Liow, J.S., Lu, J.Q., Takano, A., Model, K., Toyama, H., Suhara, T., Suzuki, K., Innis, R.B., Carson, R.E., 2003. Linearized reference tissue parametric imaging methods: application to [^{11}C]DASB positron emission tomography studies of the serotonin transporter in human brain. J. Cereb. Blood Flow Metab. 23 (9), 1096–1112.

Innis, R.B., Cunningham, V.J., Delforge, J., et al., 2007. Consensus nomenclature for in vivo imaging of reversibly binding radioligands. J. Cereb. Blood Flow Metab. 27 (9), 1533–1539.

Joshi, A., Fessler, J.A., Koeppe, R.A., 2007. Improving PET receptor binding estimates from Logan plots using principal component analysis. J. Cereb. Blood Flow Metab. 28 (4), 852–865.

Koeppe, R.A., Holthoff, V.A., Frey, K.A., Killbourn, M.R., Kuhl, D.E., 1991. Compartmental analysis of [11C]flumazenil kinetics for the estimation of ligand transport rate and receptor distribution using positron emission tomography. J. Cereb. Blood Flow Metab. 11, 735–744.

Lammertsma, A.A., Hume, S.P., 1996. Simplified reference tissue model for PET receptor studies. NeuroImage 4, 153–158.

Lammertsma, A.A., Bench, C.J., Hume, S.P., Osman, S., Gunn, K., Brooks, D.J., Frackowiak, R.S.J., 1996. Comparison of methods for analysis of clinical [^{11}C]raclopride studies. J. Cereb. Blood Flow Metab. 16, 42–52.

Logan, J., 2003. A review of graphical methods for tracer studies and strategies to reduce bias. Nucl. Med. Biol. 30 (8), 833–844.

Logan, J., Fowler, J.S., Volkow, N.D., et al., 1990. Graphical analysis of reversible radioligand binding from time-activity measurements applied to [N-11C-methuyl]-(−)-cocaine PET studies in human subjects. J. Cereb. Blood Flow Metab. 10, 740–747.

Logan, J., Fowler, J.S., Volkow, N.D., Wang, G.J., Ding, Y.S., Alexoff, D.L., 1996. Distribution volume ratios without blood sampling from graphic analysis of PET data. J. Cereb. Blood Flow Metab. 16, 834–840.

Logan, J., Fowler, J.S., Volkow, N.D., Ding, Y.S., Wang, G.J., Alexoff, D.L., 2001. A strategy for removing the bias in the graphical analysis method. J. Cereb. Blood Flow Metab. 21 (3), 307–320.

Mintun, M.A., Raichle, M.E., Killbourn, M.R., Wooten, G.F., Welch, M.J., 1984. A quantitative model for the in vivo assessment of drug binding sites with positron emission tomography. Ann. Neurol. 15, 217–227.

Ogden, R.T., 2003. Estimation of kinetic parameters in graphical analysis of PET imaging data. Stat. Med. 22 (22), 3557–3568.

Patlak, C.S., Blasberg, R.G., 1985. Graphical evaluation of blood-to-brain transfer constants from multiple-time uptake data. Generalizations. J. Cereb. Blood Flow Metab. 5, 584–590.

Patlak, C.S., Blasberg, R.G., Fenstermacher, J.D., 1983. Graphical evaluation of blood-to-brain transfer constants from multiple-time uptake data. J. Cereb. Blood Flow Metab. 3 (1), 1–7.

Slifstein, M., Laruelle, M., 2000. Effects of statistical noise on graphic analysis of PET neuroreceptor studies. J. Nucl. Med. 41, 2083–2088.

Turkheimer, F.E., Hinz, R., Cunningham, V.J., 2003. On the undecidability among kinetic models: from model selection to model averaging. J. Cereb. Blood Flow Metab. 23, 490–498.

Varga, J., Szabo, Z., 2002. Modified regression model for the Logan plot. J. Cereb. Blood Flow Metab. 22 (2), 240–244.

Wallius, E., Nyman, M., Oikonen, V., Hietala, J., Ruotsalainen, U., 2007. Voxel-based NK1 receptor occupancy measurements with [(18)F]SPA-RQ and positron emission tomography: a procedure for assessing errors from image reconstruction and physiological modeling. Mol. Imaging Biol. 9 (5), 284–294.

Wong, D.F., Wagner Jr., H.N., Dannals, R.F., et al., 1984. Effects of age on dopamine and serotonin receptors measured by positron emission tomography in the living human brain. Science 226, 1393–1396.

Wong, D.F., Gjedde, A., Wagner Jr., H.N., 1986a. Quantification of neuroreceptors in living human brain. I. Irreversible binding of ligands. J. Cereb. Blood Flow Metab. 6, 137–146.

Wong, D.F., Wagner Jr, H.N., Tune, L.E., Dannals, R.F., Pearlson, G.D., Links, J.M., Tamminga, C.A., Broussolle, E.P., Ravert, H.T., 1986b. Positron emission tomography reveals elevated D2 dopamine receptors in drug-naive schizophrenics. Science 234 (4783), 1558–1563.

Wong, D.F., Young, D., Wilson, P.D., Meltzer, C.C., Chan, B., Dannals, R.F., Ravert, H.T., Kuhar, M.J., Gjedde, A., 1997. Quantification of neuroreceptors in the living human brain: III. D2-like dopamine receptors; theory, validation and results of normal aging. J. Cereb. Blood Flow Metab. 17, 316–330.

Zhou, Y., Endres, C.J., Brasic, J.R., Huang, S.C., Wong, D.F., 2003. Linear regression with spatial constraint to generate parametric images of ligand-receptor dynamic PET studies with a simplified reference tissue model. NeuroImage 18(4), 975–989.

Zhou, Y., Resnick, S.M., Ye, W., Fan, H., Holt, D.P., Klunk, W.E., Mathis, C.A., Dannals, R., Wong, D.F., 2007a. Using a reference tissue model with spatial constraint to quantify [^{11}C]Pittsburgh compound B PET for early diagnosis of Alzheimer's disease. NeuroImage 36 (2), 291–305.

Zhou, Y., Weed, M.R., Chen, M.K., Rahmim, A., Ye, W., Brašić, J.R., Alexander, M., Crabb, A.H., McGlothan, J.L., Ali, F., Guilarte, T.R., Wong, D.F., 2007b. Quantitative dopamine transporter imaging studies in nonhuman primates with a GE Advance and high resolution research tomography (HRRT) PET scanners. J. Nucl. Med. 48 (Suppl. 2), 158P.

Zhou, Y., Resnick, S.M., Ye, W., Crabb, A.H., Wong, D.F., 2008. Using a generalized ridge regression with spatial constraint parametric imaging algorithm to improve the quantification of [^{11}C]PIB dynamic PET. J. Nucl. Med. 49 (S1), 117P.